Nanoscale

Thermally activated processes in an organic long-persistent luminescent system

Journal:	*Nanoscale*
Manuscript ID	NR-COM-12-2020-009227.R1
Article Type:	Communication
Date Submitted by the Author:	18-Feb-2021
Complete List of Authors:	Jinnai, Kazuya; Kyushu University, Center for Organic Photonics and Electronics Research (OPERA) Nishimura, Naohiro; Kyushu University, Center for Organic Photonics and Electronics Research (OPERA) Adachi, Chihaya; Kyushu University, Center for Organic Photonics and Electronics Research (OPERA) Kabe, Ryota; Okinawa Institute of Science and Technology Graduate University, Organic Optoelectronics Unit

Thermally activated processes in an organic long-persistent luminescent system

Kazuya Jinnai,[a,b] Naohiro Nishimura, [a,b] Chihaya Adachi,*[a,b,c] and Ryota Kabe*[b,d]

[a] Center for Organic Photonics and Electronics Research (OPERA), Kyushu University, 744 Motooka, Nishi-ku, Fukuoka 819-0395, Japan

[b] JST, ERATO Adachi Molecular Exciton Engineering Project, 744 Motooka, Nishi-ku, Fukuoka 819-0395, Japan

[c] International Institute for Carbon Neutral Energy Research (I2CNER), Kyushu University, 744 Motooka, Nishi-ku, Fukuoka 819-0395, Japan

[d] Organic Optoelectronics Unit, Okinawa Institute of Science and Technology Graduate University, 1919-1 Tancha, Onna-son, Kunigami-gun, Okinawa 904-0495, Japan

E-mail: ryota.kabe@oist.jp; adachi@cstf.kyushu-u.ac.jp

Abstract

Glow-in-the dark materials can store absorbed photon energy and emit light for long periods. While inorganic long-persistent luminescent (LPL) materials are crystalline and often require rare metals, organic LPL (OLPL) materials are flexible and require no rare metals. The emission process of OLPL systems consists of photo-induced charge separation, charge accumulation, and emission from charge recombination. Although emission processes of OLPL systems have been investigated, the charge separation and accumulation processes remain enigmatic. In this study, we investigated the charge carrier dynamics of a binary OLPL system comprising of electron donors and acceptors. We confirmed the presence of a thermal activation process, resembling thermally activated delayed fluorescence and thermoluminescence in the OLPL system.

1. Introduction

Glow-in-the dark materials, which can store absorbed photon energy and emit light for long periods, are currently made entirely of inorganic materials.[1,2] Inorganic long-persistent luminescent (LPL) materials are used as light sources that do not require electrical power, as in emergency signs and watch dials. Inorganic LPL materials have good luminescent properties and durability, but require various fabrication processes like powdering and dispersing into polymeric media, because of their insoluble crystalline properties. High-performance LPL materials also require rare metal dopants.[1,2]

In contrast, organic LPL (OLPL) systems,[3] consisting of organic electron donors and acceptors, do not require rare metals and can form transparent and flexible films by solution

processes[4,5]. Unlike long-lived phosphorescence,[6,7] which is a radiative transition from a triplet excited state to a singlet ground state, OLPL systems accumulate energy in charge-separated states, similar to inorganic LPL systems.[8,9] While long-lived phosphorescence shows simple exponential emission decay, the emission from charge recombination is a higher-order reaction and frequently shows emission decay according to the power-law.[10] Thus, the LPL decay is empirically fitted by the following power-law equation.[11]

$$I(t) = \frac{I_0}{(1 + At)^m} \#(1)$$ Here, A (s^{-1}) is the rate constant of the entire emission process and *m* is a parameter that depends on the materials ($0.5 < m < 2$). However, each parameter depends on the number of accumulated carriers that are affected by the emission intensity and irradiation time.[12]

The emission process of OLPL systems consists of photo-induced charge separation, charge accumulation, and emission from charge recombination. The mixture of electron donors and acceptors forms the charge-transfer (CT) excited state between them, which is called an exciplex, after photoexcitation (**Figure 1**).[13] Then, some of the CT excited states become radical ion pairs of radical cationic donors and radical anionic acceptors.[14] After successive charge recombination of these radical ion pairs, CT excited states are regenerated and emit light from the CT excited state (Fig. 1(b)).

The charge recombination process generates both singlet and triplet CT excited states of exciplexes (^{1}CT and ^{3}CT, respectively), but most of the emission is expected to occur from the radiative transition of ^{1}CT since exciplexes exhibit thermally activated delayed fluorescence (TADF) through reverse intersystem crossing (RISC) due to the small energy gap (ΔE_{ST}) between ^{1}CT and ^{3}CT.[15,16] Local triplet excited states of donors and acceptors (^{3}LE) also influence the emission process. If the ^{1}CT is the lowest excited state, LPL emission originates from the ^{1}CT, whereas if the ^{3}LE is much lower than ^{1}CT, LPL emission occurs from both ^{1}CT and ^{3}LE.[8,9]

Although emission processes of OLPL systems have been investigated, the charge separation

and accumulation processes remain to be unclarified yet. In this study, effects of excitation power intensity, excitation time, and sample temperature on photoluminescence (PL) and LPL intensities during photoexcitation were observed in order to understand the charge separation process. The initial PL process was also analyzed by time-resolved spectroscopy to understand the contribution of the charge separation process. The thermal activation process of OLPL was demonstrated by thermoluminescence (TL) measurements.

2. Experimental Section

m-MTDATA was obtained from Sigma-Aldrich (St. Louis, MA, USA). PPT was synthesized according to the literature.[17] All compounds were purified by sublimation and stored in a nitrogen-filled glovebox. The ~0.5-mm-thick mixed film was fabricated by the melt cast method. Mixtures of *m*-MTDATA (1 mol%) and PPT (99 mol%) were placed on a glass substrate with a 1-cm^2 area recessed to a depth of 0.5 mm and heated to 250 ℃ for 30 s in a nitrogen-filled glovebox. After melting, the substrate was rapidly cooled to room temperature.

For time-resolved spectroscopy studies, a pulsed Nd:YAG laser (PL2250, EKSPLA) was used as an excitation source (excitation wavelength 355 nm, pulse width 20 ps). Sample emission was detected using a gated streak camera (C10910-04, Hamamatsu Photonics). The sample was placed in a cryostat (PS-HT-200, Nagase techno-engineering) connected to a turbo molecular pump (HiPace80, Pfeiffer vacuum) and temperature was controlled from 10 K to 500 K. The sample was excited by a 355-nm pulse laser (PL2210, Ekspla) at 10 Hz.

Temperature-dependence measurements and TL measurement were conducted in a cryostat (PS-HT-200, Nagase Techno-Engineering) connected to a turbo molecular pump (HiPace 80, Pfeiffer Vacuum). Emission spectra during (steady-state photoluminescence) and after (LPL) excitation were recorded using a multichannel spectrometer (QE-Pro, Ocean Photonics). Emission decay profiles of LPL were obtained using a Silicon photomultiplier (C13366-1350GA, Hamamatsu photonics) connected to a multimeter (34461A, Keysight).

[ここに入力]

3. Results and Discussion

3.1 Photoluminescence with and without charge separation process

A mixed film of *m*-MTDATA as an electron donor, and PPT as an electron acceptor, was fabricated using a melt-cast process.[18] The sample was placed in a cryostat and was controlled from 10 K to 500 K under vacuum. The sample was photoexcited with a 355-nm pulsed laser (pulse width = 20 ps), and transient emission intensity and decay were recorded with a gated streak camera. The temperature dependence of emission decay profiles and time-resolved emission spectra are shown in **Figure 2**. Two exponential decays at nanosecond and microsecond timescales and a long emission tail of millisecond timescale were observed at room temperature (Fig. 1(a)). Emission spectra were slightly redshifted and then blueshifted over time (Fig. 1(d)), but most emission spectra are attributed to CT emission because they were broader than those of m-MTDATA and PPT (**Figure S1**). Within 10 ns after photoexcitation, the emission spectrum is slightly bluer than that of a steady-state PL spectrum due to *m*-MTDATA fluorescence, indicating insufficient CT formation.

The first exponential decay, at nanosecond timescale, corresponds to fluorescence of the exciplex, because the fluorescence lifetime (τ_p) of 350 ns is longer than that of *m*-MTDATA. The τ_p becomes longer at lower temperature due to suppression of the nonradiative decay. The second exponential decay (τ_d = 21.5 μs) corresponds to TADF, since the emission intensity increased and τ_d decreased by increasing the sample temperature (Fig. 2(f) and **Table S1**). Due to structural relaxation, the CT emission was slightly redshifted during the TADF process.[19]

The delayed emission after the TADF process corresponds to LPL emission, since the emission decay follows a power-law decay (Fig. 2(a)). Since LPL is not an exponential decay phenomenon, we cannot use the lifetime to discuss this long emission tail. The LPL emission spectra are identical to fluorescence spectra of exciplex, because the charge recombination

process generates both ^{1}CT and ^{3}CT states and the ^{3}CT excitons are upconverted to ^{1}CT. At 50 K, a power-law emission decay was observed from the microsecond timescale since the RISC process was suppressed (Fig. 2(b)). Although LPL by charge recombination is present in the whole-time scale, the LPL is difficult to observe at a short timescale, because the emission intensities of fluorescence and TADF are much stronger than that of LPL.

3.2 Charge accumulation process

Unlike long-lived phosphorescence, the charge separation process of the OLPL system requires greatly prolonged photoexcitation. LPL duration was observed by changing the photoexcitation time (**Figure 3**). LPL duration became longer and approached saturation as the excitation time increased (Fig. 3(b)). However, a slight increase was observed even with 1-hour photoexcitation, suggesting that more than 20 minutes of photoexcitation is required for sufficient charge accumulation. In the plot of excitation power intensity versus PL intensity (during photoexcitation) and integrated LPL intensity, the slope of the PL is 1, but that of LPL is close to 0.5 (Fig. 3(c)). A slope of 1 indicates a single-photon process, since fluorescence without charge separation is dominant in the PL. In contrast, a slope of 0.5 indicates that LPL intensity is proportional to the square root of excitation intensity.[20]

The charge recombination process can be considered as either geminate ion recombination,[21,22] which means recombination between the original donor-acceptor pair, or as bulk recombination,[23] which means recombination between a different donor-acceptor pair. In the steady-state, generation rates of ion pairs, g, and the charge recombination rate, $k_{CR}n^2$, are at equilibrium (k_{CR}; charge recombination rate constant, n; concentration of radical cation or radical anion). Because the generation rate of ion pairs is proportional to excitation intensity, the carrier concentration is proportional to the square root of the excitation intensity. A slope of 0.5 indicates that bulk recombination is the dominant process in this LPL emission. Previously, we reported that the LPL slope was close to 1 in the 3,3',5,5'-tetramethylbenzidine (TMB)/PPT system,[4] but

the TMB/PPT system exhibits strong room temperature phosphorescence since ^3LE_D is lower than ^1CT. Because we used the intensity at 2 s after excitation in the previous report, the contribution of room temperature phosphorescence of TMB without charge separation (one photon process, slope = 1) was significant at that time range.

To understand the charge accumulation process, time-dependent PL intensities during photoexcitation were recorded (**Figures 4 and S2**). When the excitation power was constant, PL intensity gradually increased with time, due to the increased number of molecules excited by weak photoexcitation of 1 μW (Fig. 4(a, d)). When excitation power was 10 μW, the PL intensity increased for about 100 s and then became almost constant. With the excitation power of 100 μW, the emission intensity reached its maximum in about 10 s and then decreased. Since charge accumulation is rapid at 100 μW, exciton quenching by accumulated excitons and polaron absorption by the accumulated charge is considered.[24]

When the excitation intensity is kept constant and the sample temperature is changed, the PL intensity reached its maximum in about 30 seconds and then became constant at 300 K (Fig. 4(b)). In contrast, the PL intensity quickly reached a maximum and then decreased at the low temperatures. Since charge diffusion is limited at low temperature, PL intensity saturates very quickly (**Figure 5**). At high temperatures such as 460 K, charge diffusion increases, but the effect of nonradiative deactivation also increases. Therefore, the PL intensity decreased over time. Since LPL is observed even at 10 K (Fig. 4(e)), charge recombination is thought to proceed via electron tunneling without thermal activation at low temperatures. The slope of LPL emission is nearly m = 1 at room temperature, although it varies slightly with temperature and excitation intensity. When charge recombination proceeds by random walk after de-trapping, the slope is m = 1.5, suggesting a contribution of electron tunneling, as well as thermal de-trapping.[25]

The donor/acceptor ratio is important for long-term charge accumulation, and the current optimum donor concentration is 1% for OLPL systems (Fig. 4 (f)). Although equal concentrations of donor and acceptor can form more exciplexes and are suitable for PL, charge carriers generated

by charge separation quickly recombine with neighboring donors when the donor concentration is high (Figs. 4(c), 5(c)).

3.3 Thermoluminescence

TL is often used to analyze inorganic LPL materials since the TL curve represents the trap depth of LPL systems.[26] The OLPL sample was kept at constant temperature (10, 100, 200, and 300 K) in a cryostat and photoexcited with a 340-nm LED for 300 s. After photoexcitation, the initial LPL was observed. Then, the sample temperature was increased at 5 $Kmin^{-1}$ and TL intensity was obtained. Luminescence intensity was plotted against temperature to evaluate TL behavior.

When the TL measurement of the *m*-MTDATA/PPT film was started from 10 K, a clear TL curve peaked at around 120 K was observed. This TL curve indicates the presence of a thermal activation process in the OLPL system (**Figure 6**).[27] Note that the onset of the TL curve locates at around 50 K, which is much lower than that of inorganic LPL systems. When the TL measurement was started from 300 K, a very weak TL curve peaked at around 360 K was observed. These results indicate that the most of stored charge carriers of the *m*-MTDATA/PPT film can be detrapped and recombined until it reaches at room temperature. Thus, additional trap mechanisms like a ternary OLPL system[4] are required for efficient charge trapping.

3.4 Oxygen quenching of OLPL

Because the triplet excitons of TADF systems are often quenched by molecular oxygen, optical properties were also examined under oxygen gas (**Figure 7**). As a result, the LPL emission was quenched by oxygen. Since charges accumulate in the radical cation of *m*-MTDATA and the radical anion of PPT in the LPL system, the chemical reaction of radical species with oxygen should quench LPL emission. In contrast, interestingly TADF emission was not completely quenched by oxygen due to a very thick film.

[ここに入力]

4. Conclusions

We demonstrated the presence of thermal activation and TL in an *m*-MTDATA/PPT film. The TADF process represents not only the normal TADF process without charge separation, but also LPL from charge recombination. Therefore, triplet exciton management is important for highly efficient OLPL systems, similar to TADF OLEDs.

Acknowledgments

This work was supported by the Japan Science and Technology Agency (JST), ERATO, Adachi Molecular Exciton Engineering Project, under JST ERATO Grant Number JPMJER1305, Japan, JSPS core-to-core program, and JSPS KAKENHI Grant Numbers JP18H02049 and JP18H04522. We thank K. Kusuhara and N. Nakamura for their assistance with the preparation of PPT.

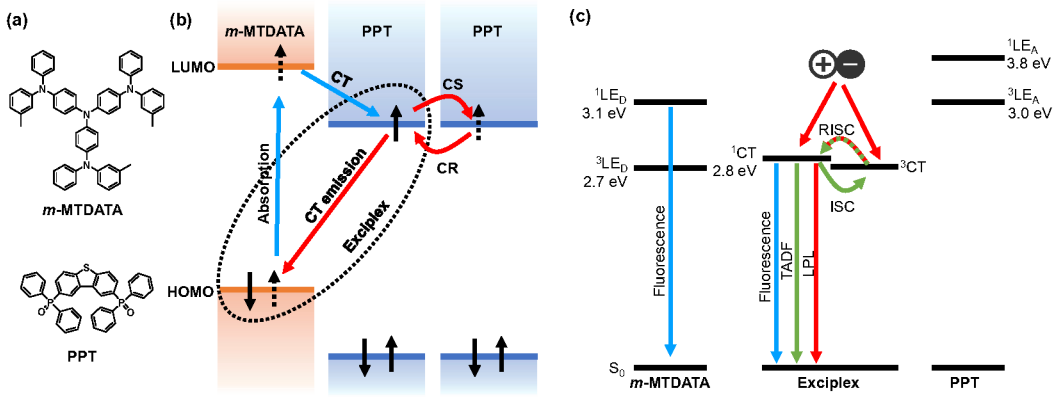

Figure 1. (a) Chemical structures of the electron donor, *m*-MTDATA, and the acceptor, PPT. (b) HOMO and LUMO energy diagrams and the emission mechanism of an OLPL system. (c) Singlet and triplet energy diagram of an *m*-MTDATA/PPT system. The OLPL system exhibits fluorescence, TADF, and LPL from the ^{1}CT state.

[ここに入力]

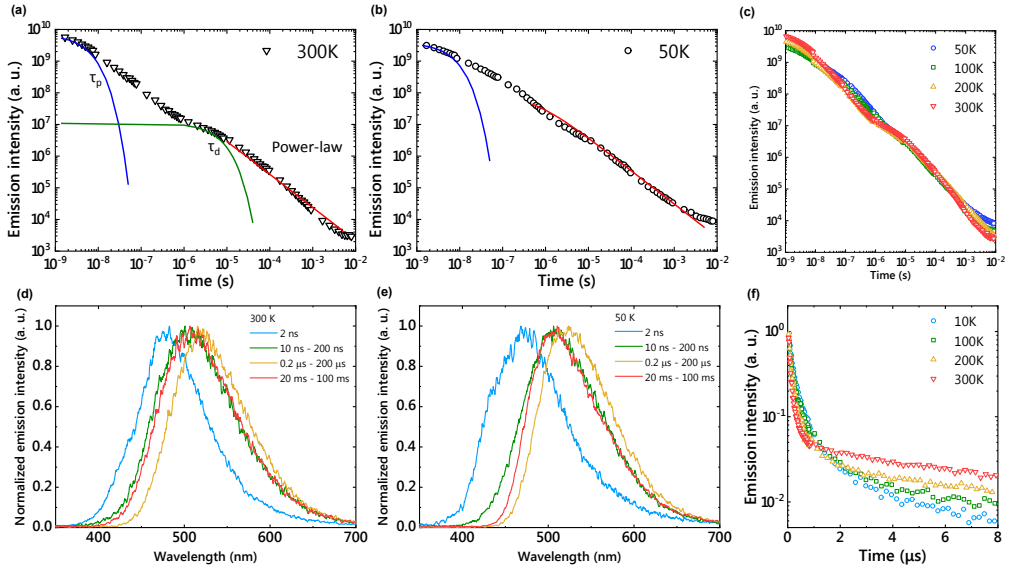

Figure 2. Emission decay profiles in a log-log plot of *m*-MTDATA/PPT film at 300 K (a), 50 K (b), and various temperatures (c). Solid lines show fitting of τ_P, τ_d, and power-law decay. Time-dependent emission spectra at 300 K (d) and 50 K (e). Emission decay profiles in a semi-log plot (f).

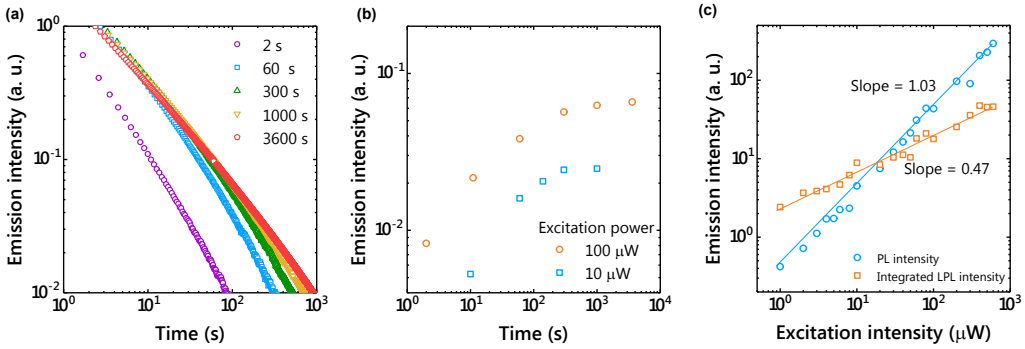

Figure 3. (a) Emission decay profiles showing the dependence of LPL on excitation time (1 molar ratio of the donor; excitation power, 100 μW; temperature, 300 K). (b) Excitation-time dependence of emission intensity 100 s after photoexcitation. (c) Excitation-power dependence of emission intensity under photoexcitation (PL) and integrated LPL intensity. LPL intensity was integrated from 100 s to 10000 s after photoexcitation. The solid lines show liner fitting.

[ここに入力]

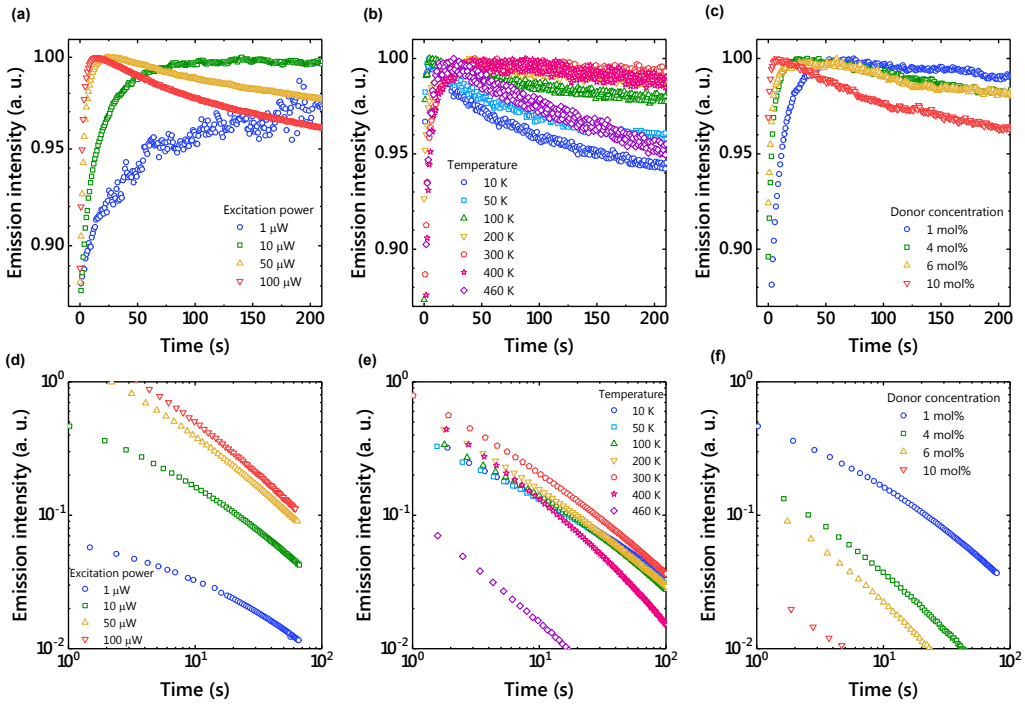

Figure 4. (a) Excitation power dependence of time-dependent emission intensity under photoexcitation (1 molar ratio of the donor; temperature, 300 K). (b) Temperature dependence of time-dependent emission intensity under photoexcitation (1 molar ratio of the donor; excitation power, 10 μW). (c) Donor concentration dependence of time-dependent emission intensity under photoexcitation (excitation power, 10 μW; temperature, 300 K). (d) Excitation power dependence of time-dependent emission intensity after photoexcitation (1 molar ratio of the donor; temperature, 300 K). (e) Temperature dependence of time-dependent emission intensity after photoexcitation (1 molar ratio of the donor; excitation power, 10 μW). (f) Donor concentration dependence of time-dependent emission intensity after photoexcitation (excitation power, 10 μW; temperature, 300 K).

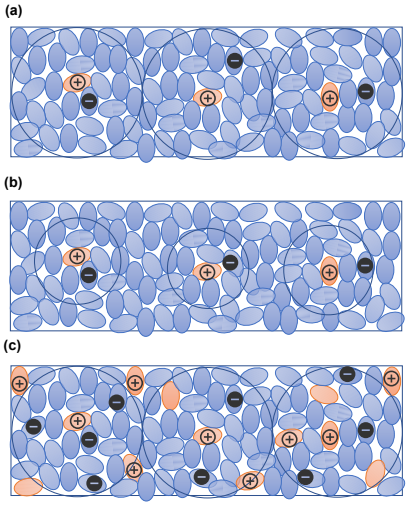

[ここに入力]

Figure 5. (a) Schematic diagram of a donor/acceptor mixed film. Charge separation occurs at the interface between electron donors and acceptors. Due to the low donor concentration, holes are localized to the donors and electrons diffuse to neighboring acceptor molecules. (b) Schematic diagram of charge separation at low temperature. Electrons can diffuse shorter distances at low temperature. (c) Schematic diagram of charge separation at a higher doping concentration. Generated charges quickly recombine with neighboring donors.

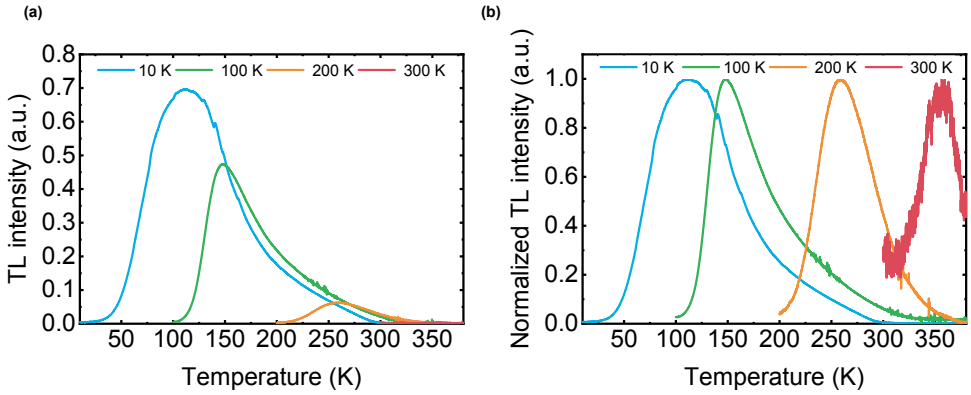

Figure 6. (a) TL curves of an *m*-MTDATA/PPT film. Sample was photoexcited at the starting temperature (10 K, 100 K, 200 K, and 300 K) for 300 s. After 1 h, sample temperature was increased at 5 $Kmin^{-1}$. (b) Normalized TL curves.

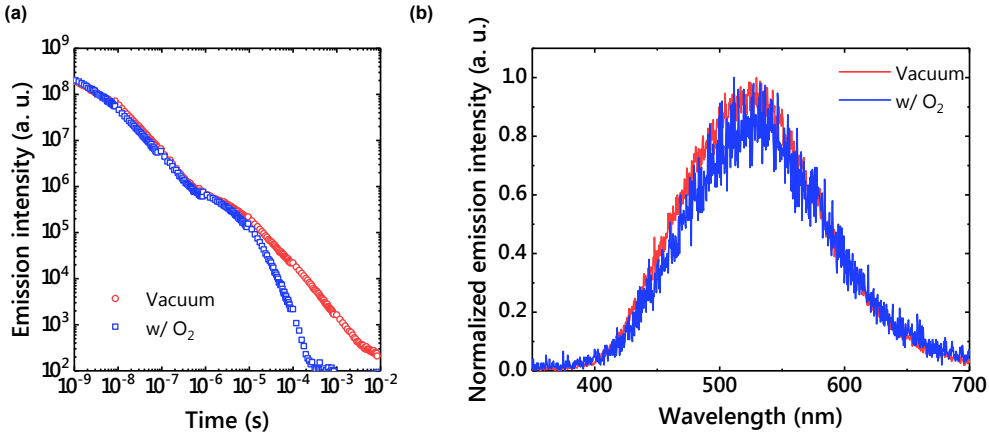

Figure 7. (a) An emission decay profile under vacuum and in air. The power-law decay disappeared in air. (b) Delayed emission spectra under vacuum and in air.

[ここに入力]

References

1. J. Xu and S. Tanabe, *J. Lumin.*, 2019, **205**, 581.
2. S. Wu, Z. Pan, R. Chen and X. Liu, *Long Afterglow Phosphorescent Materials*, Springer International Publishing, Cham, 2017.
3. R. Kabe and C. Adachi, Nature, 2017, **550**, 384.
4. K. Jinnai, R. Kabe and C. Adachi, Adv. Mater., 2018, **30**, 1800365.
5. Z. Lin, R. Kabe, N. Nishimura, K. Jinnai and C. Adachi, Adv. Mater., 2018, **30**, 1803713.
6. S. Hirata, Adv. Opt. Mater., 2017, **5**, 1700116.
7. Kenry, C. Chen and B. Liu, Nat. Commun., 2019, **10**, 2111.
8. N. Nishimura, Z. Lin, K. Jinnai, R. Kabe and C. Adachi, Adv. Funct. Mater., 2020, **30**, 2000795.
9. Z. Lin, R. Kabe, K. Wang and C. Adachi, Nat. Commun., 2020, **11**, 191.
10. D. Hertel, H. Bässler, R. Guentner and U. Scherf, J. Chem. Phys., 2001, **115**, 10007.
11. H. Ohkita, W. Sakai, A. Tsuchida and M. Yamamoto, Bull. Chem. Soc. Jpn., 1997, **70**, 2665.
12. K. Gouda and Y. Hama, Radiat. Phys. Chem., 1985, **26**, 285.
13. M. Sarma and K.-T. Wong, ACS Appl. Mater. Interfaces, 2018, **10**, 19279.
14. T. M. Clarke and J. R. Durrant, Chem. Rev., 2010, **110**, 6736.
15. K. Goushi, K. Yoshida, K. Sato and C. Adachi, Nat. Photonics, 2012, **6**, 253.
16. H. Noda, X.-K. Chen, H. Nakanotani, T. Hosokai, M. Miyajima, N. Notsuka, Y. Kashima, J.-L. Brédas and C. Adachi, Nat. Mater., 2019, **18**, 1084.
17. C. Fan, C. Duan, Y. Wei, D. Ding, H. Xu and W. Huang, Chem. Mater. 2015, **27**, 5131
18. K. Jinnai, N. Nishimura, R. Kabe and C. Adachi, Chem. Lett., 2019, **48**, 270.
19. T. -C. Lin, M. Sarma, Y. -T. Chen, S. -H. Liu, K. -T. Lin, P. -Y. Chiang, W. -T. Chuang, Y. -C. Liu, H. -F. Hsu, W. -Y. Hung, W. -C. Tang, K. -T. Wong, and P. -T. Chou, Nat. Commun., 2018, **9**, 3111.
20. K. Seki, K. Marumoto, and M. Tachiya, Appl. Phys. Express, 2013, **6**, 051603.
21. M. Wojcik, A. Nowak and K. Seki, J. Chem. Phys., 2017, **146**, 054101.
22. K. Seki, K. Murayama and M. Tachiya, Phys. Rev. B, 2005, **71**, 235212.
23. J. S. Manser and P. V. Kamat, Nat. Photonics, 2014, **8**, 737.
24. D. Jia, Opt. Mater., 2003, **22**, 65.
25. M. Tachiya and K. Seki, Appl. Phys. Lett., 2009, **94**, 081104.
26. K. Van den Eeckhout, P. F. Smet and D. Poelman, Materials, 2010, **3**, 2536.
27. J. Ueda, K. Kuroishi, and S. Tanabe, Appl. Phys. Lett., 2014, **104**, 101904

[ここに入力]